Journal of
Mechanics of
Materials and Structures

LONG WAVELENGTH BIFURCATIONS AND MULTIPLE NEUTRAL AXES OF ELASTIC LAYERED STRUCTURES SUBJECT TO FINITE BENDING

Sara Roccabianca, Davide Bigoni and Massimiliano Gei

Volume 6, No. 1-4 January–June 2011

mathematical sciences publishers

JOURNAL OF MECHANICS OF MATERIALS AND STRUCTURES
Vol. 6, No. 1-4, 2011

LONG WAVELENGTH BIFURCATIONS AND MULTIPLE NEUTRAL AXES OF ELASTIC LAYERED STRUCTURES SUBJECT TO FINITE BENDING

SARA ROCCABIANCA, DAVIDE BIGONI AND MASSIMILIANO GEI

Dedicated to Marie-Louise and Charles Steele

Geometries and rigidities involving the presence of more than one neutral axis during finite (plane-strain) bending of a multilayered elastic (incompressible) block make numerically stiff the differential equations governing the incremental problem necessary to investigate diffuse-mode instabilities. We have developed a compound matrix method to solve these cases, so that we have shown that the presence of two neutral axes occurs within sets of parameters where the elastic system may display long-wavelength bifurcation modes. Following the predictions of the theory, we have designed and realized qualitative experiments in which these modes become visible.

1. Introduction

Recently Roccabianca et al. [2010] have addressed, solved and experimented the problem of bifurcation of a layered incompressible elastic block, subject to finite bending in plane strain. They were able to show that a layered system exhibits bifurcation loads and angles of bending completely different from those occurring in a uniform elastic block. They found that for several geometries and stiffness contrasts the first ("critical") bifurcation load corresponds to a long-wavelength mode, which results to be very close to the bifurcation load associated with the surface instability limit of vanishing wavelength,[1] a feature also common to the behavior of a uniform elastic block. This feature explains the experimental observation (on uniform blocks [Gent and Cho 1999; Gent 2005] and bilayers [Roccabianca et al. 2010]) that short-wavelength modes become visible, instead of the long-wavelength modes that are predicted to occur before. Therefore, the question was left open whether or not wavelength modes longer than the short-wavelength modes available at surface instability and visible in the experiments can be experimentally displayed with a layered system in which an appropriate selection is made of stiffness and thickness contrasts between layers. We provide a positive answer to this problem in the present article, so that our calculations, based now on the compound matrix method [Backus and Gilbert 1967; Ng and Reid 1979a;

Financial support of PRIN grant no. 2007YZ3B24 "Multiscale Problems with Complex Interactions in Structural Engineering" financed by Italian Ministry of University and Research is gratefully acknowledged. Experiments have been conducted by S. R. at the Laboratory for Physical Modeling of Structures and Photoelasticity of the University of Trento, managed by D. B.; see http://www.ing.unitn.it/dims/ssmg.

Keywords: nonlinear elasticity, neutral axis, instability, composite plate, compound matrix method.

[1] Surface instability occurs in a uniformly strained half space as a bifurcated mode of arbitrary wavelength, corresponding to a Rayleigh wave of vanishing speed. In the limit of vanishing wavelength, surface instability can be viewed as a bifurcation mode adaptable to every boundary and state of stress of a strained body, so that it becomes a local instability mode (also called "failure of the complementing condition" in [Benallal et al. 1993]).

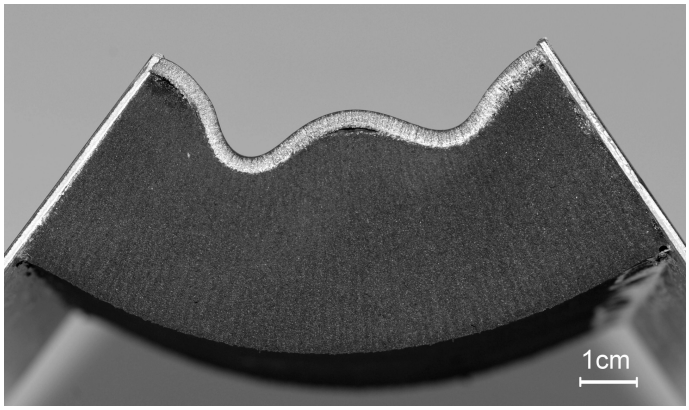

Figure 1. Bifurcation of a two-layer rubber block under finite bending evidencing long-wavelength bifurcation modes. Stiffness and thickness ratios between the layers are $(2.687\,\mathrm{N/mm^2})/(0.095\,\mathrm{N/mm^2})$ and $(3\,\mathrm{mm})/(40\,\mathrm{mm})$. The stiff layer ($86\,\mathrm{mm} \times 3\,\mathrm{mm} \times 150\,\mathrm{mm}$, made up of natural rubber, marked with a white pencil on the sample) is at the compressive side and coats a neoprene layer ($86\,\mathrm{mm} \times 40\,\mathrm{mm} \times 150\,\mathrm{mm}$).

1979b; 1985], allow us to conclude that there are situations in which the long-wavelength modes are well-separated from the surface instability, so that systems exhibiting bifurcation modes of long wavelength can be designed. These systems have been realized by us and qualitatively tested, showing that the theory predictions are generally followed, Figure 1.

It turns out that the hunt for long-wavelength modes can be related[2] to the presence of more than one neutral axis (namely, the line of null normal stresses) during bending, an issue that was noted in [Roccabianca et al. 2010], but not investigated in detail.

In a bilayer, two neutral axes typically occur when a stiff layer is placed at the compressive side of the system, a case in which the differential equations become numerically stiff, so that we have employed an ad hoc version of the compound matrix method, which is shown to allow systematic investigation of the situations in which more than one neutral axis occurs. In these cases we find a sort of inversion of the sequence of bifurcation modes with the aspect ratio of the system, so that high-wavenumber modes are relevant for lower slender ratios than small-wavenumber modes.

2. Finite bending of an elastic multilayer and incremental bifurcations

We review the theory developed in [Roccabianca et al. 2010] for finite bending of an elastic incompressible multilayered block and for incremental bifurcations, both addressed here only in the special case of a Mooney–Rivlin material,[3] a choice which affects results, but simplifies the treatment.

We denote a generic layer with a superscript (s) ($s = 1, \ldots, N$), so that, in the reference stress-free configuration, a Cartesian coordinate system $O_0^{(s)} x_1^{0(s)} x_2^{0(s)} x_3^{0(s)}$ is introduced for each layer, centered at

[2] The relation is that within the parameter range in which long-wavelength bifurcations occur well-separated from surface instability, two neutral axes are often found.

[3] Bending of an elastic homogeneous block has been solved in [Rivlin 1949], while incremental bifurcations have been analyzed in [Triantafyllidis 1980; Dryburgh and Ogden 1999; Coman and Destrade 2008; Destrade et al. 2009; 2010].

its centroid, with basis vectors $\boldsymbol{e}_i^0$ $(i = 1, 2, 3)$, $x_1^{0(s)} \in [-h_0^{(s)}/2, h_0^{(s)}/2]$, $x_2^{0(s)} \in [-l_0/2, l_0/2]$, and with $x_3^{0(s)}$ denoting the out-of-plane coordinate.

The deformed configuration of each layer is a sector of a cylindrical tube of half-angle $\bar{\theta}$, so that it becomes convenient to introduce a cylindrical coordinate system $O^{(s)}r^{(s)}\theta^{(s)}z^{(s)}$, with basis vectors $\boldsymbol{e}_r$, $\boldsymbol{e}_\theta$ and $\boldsymbol{e}_z$, $r^{(s)} \in [r_i^{(s)}, r_i^{(s)} + h^{(s)}]$, $\theta^{(s)} \in [-\bar{\theta}, +\bar{\theta}]$, and with out-of-plane coordinate $z^{(s)}$.

The imposition of incompressibility (conservation of volume) yields

$$r_i^{(s)} = \frac{l_0 h_0^{(s)}}{2\bar{\theta} h^{(s)}} - \frac{h^{(s)}}{2}, \tag{1}$$

where $h^{(s)}$ is the current thickness of the s–th layer. Following [Roccabianca et al. 2010], the imposition of the incompressibility constraint in terms of principal stretches (λ_r, λ_θ and λ_z) and of the boundary conditions at $x_2^{0(s)} = \pm l_0/2$ and $x_1^{0(s)} = -h_0^{(s)}/2$ provides

$$\lambda_r^{(s)} = \frac{1}{\alpha r^{(s)}}, \quad \lambda_\theta^{(s)} = \alpha r^{(s)}, \quad \lambda_z^{(s)} = 1, \tag{2}$$

where $\alpha = 2\bar{\theta}/l_0$; note that α is independent of index s.

The N layers forming the multilaminated structure are assumed to be perfectly bonded to each other, so that

$$r_i^{(s)} = r_i^{(s-1)} + h^{(s-1)} \quad (s = 2, \ldots, N), \tag{3}$$

where $r_i^{(s)}$ is given by (1). Condition (3) provides all thicknesses $h^{(s)}$ $(s = 2, \ldots, N)$ as a function of the thickness of the first layer $h^{(1)}$, remaining the sole kinematical unknown of the problem, to be determined as the solution of the boundary-value problem.

Since the layers are assumed to be perfectly bonded, all radial coordinates $r^{(s)}$ can be referred to the same origin O of a cylindrical coordinate system $Or\theta z$, common to all deformed layers; therefore, the index s will be omitted in the following in all coordinates and the deformed configuration will be described in terms of the global system $Or\theta z$.

Finally, the kinematics provides all stretches in the multilayer which can be represented as

$$\lambda_r = \frac{1}{\lambda} = \frac{l_0}{2\bar{\theta} r}, \quad \lambda_\theta = \lambda = \frac{2\bar{\theta} r}{l_0}, \quad \lambda_z = 1, \tag{4}$$

and the current thickness of the s–th layer, $h^{(s)}$, as a function of $h^{(s-1)}$, namely

$$h^{(s)} = -\frac{l_0 h_0^{(s-1)}}{2\bar{\theta} h^{(s-1)}} - \frac{h^{(s-1)}}{2} + \sqrt{\left(\frac{l_0 h_0^{(s-1)}}{2\bar{\theta} h^{(s-1)}} + \frac{h^{(s-1)}}{2}\right)^2 + \frac{l_0 h_0^{(s)}}{\bar{\theta}}} \quad (s = 2, \ldots, N), \tag{5}$$

determining all current thicknesses as functions of the thickness of the first layer, $h^{(1)}$ (in [Roccabianca et al. 2010, Equation (21)], corresponding to our (5), a minus sign appears by mistake instead of a plus in front of the last term under the square root).

A constitutive prescription between the principal components of the Cauchy stress T_i $(i = 1, 2, 3)$ and the principal stretches λ_i $(i = 1, 2, 3)$ can be written as

$$T_i = -\pi + \lambda_i \frac{\partial W(\lambda_1, \lambda_2, \lambda_3)}{\partial \lambda_i}, \quad \lambda_1\lambda_2\lambda_3 = 1, \tag{6}$$

where the index i is not summed and π is an arbitrary Lagrangian multiplier representing the undetermined hydrostatic pressure.

For a generic layer s, the Cauchy stress can be represented in polar coordinates as

$$\boldsymbol{T}^{(s)} = T_r^{(s)} \boldsymbol{e}_r \otimes \boldsymbol{e}_r + T_\theta^{(s)} \boldsymbol{e}_\theta \otimes \boldsymbol{e}_\theta + T_z^{(s)} \boldsymbol{e}_z \otimes \boldsymbol{e}_z, \tag{7}$$

and calculated from the constitutive equations (6). Here, we adopt the Mooney–Rivlin strain-energy function defined in terms of the moduli c_1 and c_2 and of the left Cauchy–Green deformation tensor $\boldsymbol{B}$ as (for layer s)

$$W^{(s)} = \frac{c_1^{(s)}}{2}(\operatorname{tr} \boldsymbol{B} - 3) + \frac{c_2^{(s)}}{2}(\operatorname{tr} \boldsymbol{B}^{-1} - 3). \tag{8}$$

For a plane-strain deformation, defining the shear modulus μ_0 as

$$\mu_0^{(s)} = c_1^{(s)} + c_2^{(s)}, \tag{9}$$

the integration of the equilibrium equation ($\operatorname{div} \boldsymbol{T} = \boldsymbol{0}$) within each layer yields, for the components of Cauchy stress,

$$\begin{aligned} T_r^{(s)} &= \hat{W}^{(s)} + \gamma^{(s)} = \frac{\mu_0^{(s)}}{2}\left(\lambda^2 + \frac{1}{\lambda^2}\right) + \gamma^{(s)}, \\ T_\theta^{(s)} &= \left(\lambda \hat{W}^{(s)}\right)' + \gamma^{(s)} = \frac{\mu_0^{(s)}}{2}\left(3\lambda^2 - \frac{1}{\lambda^2}\right) + \gamma^{(s)}, \end{aligned} \tag{10}$$

where $\hat{W}^{(s)}(\lambda) = W^{(s)}(1/\lambda, \lambda, 1)$, $\gamma^{(s)}$ is an integration constant, and $()'$ denotes differentiation with respect to the stretch λ. The component $T_z^{(s)}$ can be inferred from (6). Note that in plane strain, the definition of W in (8) specializes to

$$W^{(s)} = \frac{c_1^{(s)} + c_2^{(s)}}{2}\left(\lambda^2 + \frac{1}{\lambda^2} - 2\right) = \frac{\mu_0^{(s)}}{2}\left(\lambda^2 + \frac{1}{\lambda^2} - 2\right). \tag{11}$$

The N constants $\gamma^{(s)}$ can be determined by imposing the boundary conditions at the external sides of the layered system, namely

$$T_r^{(1)}(r_i^{(1)}) = 0, \quad T_r^{(N)}(r_e^{(N)}) = 0, \tag{12}$$

and the interfacial continuity conditions

$$T_r^{(s-1)}(r_e^{(s-1)}) = T_r^{(s)}(r_i^{(s)}) \quad (s = 2, \ldots, N), \tag{13}$$

where $r_e^{(s-1)} = r_i^{(s-1)} + h^{(s-1)}$ $(s = 2, \ldots, N + 1)$. In particular, the constant $\gamma^{(N)}$ can be calculated from $(12)_2$ using $(10)_1$ as

$$\gamma^{(N)} = -\frac{\mu_0^{(N)}}{2}\left[(\alpha r_e^{(N)})^2 + \frac{1}{(\alpha r_e^{(N)})^2}\right], \tag{14}$$

while from (13) the following recursion rule, useful in computing all the remaining constants $\gamma^{(s)}$, can be inferred

$$\gamma^{(s-1)} = \frac{\mu_0^{(s)} - \mu_0^{(s-1)}}{2}\left[(\alpha r_e^{(s-1)})^2 + \frac{1}{(\alpha r_e^{(s-1)})^2}\right] + \gamma^{(s)} \quad (s = 2, \ldots, N), \tag{15}$$

where $r_i^{(s)} = r_e^{(s-1)}$. In the special case $N = 2$, (15) and $(12)_1$ provide

$$\frac{\mu_0^{(1)}}{2}\left[(\alpha r_i^{(1)})^2 + \frac{1}{(\alpha r_i^{(1)})^2}\right] + \frac{\mu_0^{(2)} - \mu_0^{(1)}}{2}\left[(\alpha r_e^{(1)})^2 + \frac{1}{(\alpha r_e^{(1)})^2}\right] + \gamma^{(2)} = 0, \tag{16}$$

in which $r_i^{(1)}$, $r_e^{(1)}$ and $\gamma^{(2)}$ are all functions of $h^{(1)}$, through (1), (5), and (15). Therefore, (16) can be numerically solved to obtain the current thickness of the first layer, $h^{(1)}$, which determines the solution of a bilayer subject to finite bending.

Now that the bending solution is known, this can be used as the fundamental solution in an analysis of incremental bifurcations. The incremental equilibrium is expressed in terms of the updated incremental first Piola–Kirchhoff stress $\boldsymbol{\Sigma}$ by

$$\operatorname{div} \boldsymbol{\Sigma} = \mathbf{0}, \tag{17}$$

where

$$\boldsymbol{\Sigma} = \dot{\boldsymbol{S}}\boldsymbol{F}^T, \quad \dot{\boldsymbol{S}} = \dot{\boldsymbol{T}}\boldsymbol{F}^{-T} - \boldsymbol{T}\boldsymbol{L}^T\boldsymbol{F}^{-T}, \tag{18}$$

$\boldsymbol{S} = \boldsymbol{T}\boldsymbol{F}^{-T}$ and a superposed dot is used to denote a first-order increment. $\boldsymbol{L}$ is the gradient of incremental displacements with cylindrical components

$$\boldsymbol{L} = u_{r,r}\boldsymbol{e}_r \otimes \boldsymbol{e}_r + \frac{u_{r,\theta} - u_\theta}{r}\boldsymbol{e}_r \otimes \boldsymbol{e}_\theta + u_{\theta,r}\boldsymbol{e}_\theta \otimes \boldsymbol{e}_r + \frac{u_r + u_{\theta,\theta}}{r}\boldsymbol{e}_\theta \otimes \boldsymbol{e}_\theta, \tag{19}$$

subject to the constraint $\operatorname{tr} \boldsymbol{L} = 0$ (incremental incompressibility), namely,

$$r u_{r,r} + u_r + u_{\theta,\theta} = 0. \tag{20}$$

The linearized constitutive equation is

$$\boldsymbol{\Sigma} = \mathbb{C}\boldsymbol{L} - \dot{\pi}\boldsymbol{I}, \tag{21}$$

where $\mathbb{C}$ is the fourth-order tensor of instantaneous elastic moduli and, since $\boldsymbol{\Sigma} = \dot{\boldsymbol{T}} - \boldsymbol{T}\boldsymbol{L}^T$ [see (18)], the balance of rotational momentum yields

$$\Sigma_{12} - \Sigma_{21} = T_2 L_{12} - T_1 L_{21}, \tag{22}$$

so that

$$\mathbb{C}_{ijji} + T_i = \mathbb{C}_{jiji} \quad (i \neq j), \tag{23}$$

where the indices i and j are not summed.

For an incompressible isotropic elastic material, the components of $\mathbb{C}$ can be written as functions of two incremental moduli, denoted by μ and μ_*, that depend on the current deformation. In cylindrical

coordinates, the nonvanishing components of $\mathbb{C}$ are (see [Hill and Hutchinson 1975; Gei and Ogden 2002])

$$\begin{aligned} &C_{rrrr} = C_{\theta\theta\theta\theta} = 2\mu_* + p, \quad C_{\theta r\theta r} = \mu - \Gamma, \\ &C_{r\theta r\theta} = \mu + \Gamma, \qquad\qquad C_{r\theta\theta r} = C_{\theta rr\theta} = \mu + p, \end{aligned} \tag{24}$$

where

$$\Gamma = \frac{T_\theta - T_r}{2} \quad \text{and} \quad p = -\frac{T_\theta + T_r}{2}, \tag{25}$$

describe the state of prestress. Hence, the incremental constitutive equations (21) take the explicit form

$$\begin{aligned} &\Sigma_{rr} = -\dot\pi + (2\mu_* + p)u_{r,r}, \qquad\qquad \Sigma_{\theta\theta} = -\dot\pi + (2\mu_* + p)\frac{u_r + u_{\theta,\theta}}{r}, \\ &\Sigma_{r\theta} = (\mu + \Gamma)\frac{u_{r,\theta} - u_\theta}{r} + (\mu + p)u_{\theta,r}, \quad \Sigma_{\theta r} = (\mu + p)\frac{u_{r,\theta} - u_\theta}{r} + (\mu - \Gamma)u_{\theta,r}. \end{aligned} \tag{26}$$

For a Mooney–Rivlin material deformed in plane strain, the two moduli μ and μ_* coincide and are equal to [see (8)]

$$\mu = \mu_* = \frac{\mu_0}{2}\frac{(\lambda^4 + 1)}{\lambda^2}. \tag{27}$$

We seek bifurcation represented by an incremental displacement field in the form

$$\begin{cases} u_r(r,\theta) = f(r)\cos n\theta, \\ u_\theta(r,\theta) = g(r)\sin n\theta, \\ \dot\pi(r,\theta) = k(r)\cos n\theta, \end{cases} \tag{28}$$

so that (20) can be reformulated as

$$g = -\frac{(f + rf')}{n}, \tag{29}$$

and the incremental equilibrium equations as

$$\begin{aligned} k' &= Df'' + \left(C_{,r} + D_{,r} + \frac{C + 2D}{r}\right)f' + \frac{E(1 - n^2)}{r^2}f, \\ k &= \frac{r^2 C}{n^2}f''' + \frac{F + 3C}{n^2}rf'' + \left(\frac{F}{n^2} - D\right)f' - \frac{1 - n^2}{n^2}\frac{F}{r}f, \end{aligned} \tag{30}$$

where coefficients C, D, E and F can be expressed (for a Mooney–Rivlin material) as

$$\begin{aligned} &C = \mu - \Gamma = \frac{\mu_0}{\lambda^2}, \qquad D = 2\mu_* - \mu = \frac{\mu_0}{2}\frac{\lambda^4 + 1}{\lambda^2}, \\ &E = \mu + \Gamma = \mu_0\lambda^2, \quad F = rC_{,r} + C = -\frac{\mu_0}{\lambda^2}. \end{aligned} \tag{31}$$

By differentiating $(30)_2$ with respect to r and substituting the result into $(30)_1$, a single differential equation in terms of $f(r)$ is obtained:

$$r^4 f'''' + 2r^3 f''' - \big(3 + n^2(\lambda^4 + 1)\big)r^2 f'' + \big(3 + n^2(1 - 3\lambda^4)\big)rf' + (n^2 - 1)(3 + n^2\lambda^4)f = 0, \tag{32}$$

defining the function $f(r)$ within a generic layer. Once $f(r)$ is known for each layer, the other functions, $g(r)$ and $k(r)$, can be calculated by employing (29) and $(30)_2$, respectively, so that function $f(r)$ becomes the primary unknown.

The differential equation (32) for the functions $f^{(s)}(r)$ $(s = 1, \dots, N)$ is complemented by the following boundary conditions:

- continuity of incremental tractions and displacements across interfaces:

$$\begin{aligned}
&f^{(s)}\big|_{r=r_e^{(s)}} = f^{(s+1)}\big|_{r=r_i^{(s+1)}},\\
&\{f+rf'\}^{(s)}\Big|_{r=r_e^{(s)}} = \{f+rf'\}^{(s+1)}\Big|_{r=r_i^{(s+1)}},\\
&\Big\{\mu_0\Big(r^3f'''+2r^2f''-\big(1+n^2\big(\tfrac{1}{2}(3+\lambda^4)-\bar\gamma\big)\big)rf'+(1-n^2)f\Big)\Big\}^{(s)}\Big|_{r=r_e^{(s)}} =\\
&\Big\{\mu_0\Big(r^3f'''+2r^2f''-\big(1+n^2\big(\tfrac{1}{2}(3+\lambda^4)-\bar\gamma\big)\big)rf'+(1-n^2)f\Big)\Big\}^{(s+1)}\Big|_{r=r_i^{(s+1)}},\\
&\Big\{\mu_0\Big(r^2f''+\big(\tfrac{1}{2}(3+\lambda^4)+\bar\gamma\big)rf'+(1-n^2)\big(\tfrac{1}{2}(\lambda^4-1)+\bar\gamma\big)f\Big)\Big\}^{(s)}\Big|_{r=r_e^{(s)}} =\\
&\Big\{\mu_0\Big(r^2f''+\big(\tfrac{1}{2}(3+\lambda^4)+\bar\gamma\big)rf'+(1-n^2)\big(\tfrac{1}{2}(\lambda^4-1)+\bar\gamma\big)f\Big)\Big\}^{(s+1)}\Big|_{r=r_i^{(s+1)}},
\end{aligned} \tag{33}$$

  where $\bar\gamma^{(s)} = \gamma^{(s)}\lambda^2/\mu_0^{(s)}$;

- null tractions (for dead loading) at the external surfaces ($r = r_i^{(1)}$ and $r = r_e^{(N)}$):

$$\begin{aligned}
&\big\{r^3f'''+2r^2f''-\big(1+n^2(2+\lambda^4)\big)rf'+(1-n^2)f\big\}^{(1),(N)}\Big|_{r=r_i^{(1)},r_e^{(N)}}=0,\\
&\big\{r^2f''+rf'+(n^2-1)f\big\}^{(1),(N)}\Big|_{r=r_i^{(1)},r_e^{(N)}}=0;
\end{aligned} \tag{34}$$

- null incremental normal displacement and nominal shear stress (at $\theta = \pm\bar\theta$), which yields

$$n = \frac{2m\pi}{\alpha l_0} \quad (m = 1, 2, 3, \dots). \tag{35}$$

3. The compound matrix method for a bilayer

The compound matrix method was initially proposed in [Backus and Gilbert 1967] and applied to problems of fluid mechanics [Backus and Gilbert 1967; Ng and Reid 1979a; 1979b; 1985, Anturkar et al. 1992; Yiantsios and Higgins 1988] and solid mechanics [Lindsay 1992; Lindsay and Rooney 1992]. Haughton and Orr [1995] used the method in incremental elasticity, while Haughton [1999], Dryburgh and Ogden [1999] and Destrade et al. [2009; 2010] employed it to investigate instabilities of a homogeneous block subjected to finite flexure. Our aim is to show the application to elastic multilayers subject to finite bending, in the simple case of a bilayer.

The differential equation (32) can be rewritten as a linear system of first-order ODEs, that in the case of two elastic layers can be cast in the standard form

$$\boldsymbol{y}' = \boldsymbol{A}\boldsymbol{y}, \quad \boldsymbol{z}' = \boldsymbol{B}\boldsymbol{z}, \tag{36}$$

where the vectors $\boldsymbol{y}$ and $\boldsymbol{z}$ are defined as

$$\begin{aligned} \boldsymbol{y}(r) &= \left[f^{(1)}(r) \;\; f^{(1)\prime}(r) \;\; f^{(1)\prime\prime}(r) \;\; f^{(1)\prime\prime\prime}(r) \right]^T, \\ \boldsymbol{z}(r) &= \left[f^{(2)}(r) \;\; f^{(2)\prime}(r) \;\; f^{(2)\prime\prime}(r) \;\; f^{(2)\prime\prime\prime}(r) \right]^T, \end{aligned} \tag{37}$$

and the matrices $\boldsymbol{A}$ and $\boldsymbol{B}$, which depend on the radial coordinate r, as

$$\boldsymbol{A}(r) = \begin{bmatrix} 0 & 1 & 0 & 0 \\ 0 & 0 & 1 & 0 \\ 0 & 0 & 0 & 1 \\ A_{41} & A_{42} & A_{43} & A_{44} \end{bmatrix}, \quad \boldsymbol{B}(r) = \begin{bmatrix} 0 & 1 & 0 & 0 \\ 0 & 0 & 1 & 0 \\ 0 & 0 & 0 & 1 \\ B_{41} & B_{42} & B_{43} & B_{44} \end{bmatrix}. \tag{38}$$

The components of $\boldsymbol{A}$ and $\boldsymbol{B}$, as well as those of other matrices and vectors introduced in this Section are listed in Appendix A.

The boundary conditions at the two external surfaces of the layer, equations (34), are equivalent to

$$\boldsymbol{C}\boldsymbol{y}(r_i) = \boldsymbol{0}, \quad \boldsymbol{D}\boldsymbol{z}(r_e) = \boldsymbol{0}, \tag{39}$$

where $r_i = r_i^{(1)}$, $r_e = r_i^{(2)} + h^{(2)}$ and matrices $\boldsymbol{C}$ and $\boldsymbol{D}$ are

$$\boldsymbol{C} = \begin{bmatrix} C_{11} & C_{12} & C_{13} & C_{14} \\ C_{21} & C_{22} & C_{23} & 0 \end{bmatrix}, \quad \boldsymbol{D} = \begin{bmatrix} D_{11} & D_{12} & D_{13} & D_{14} \\ D_{21} & D_{22} & D_{23} & 0 \end{bmatrix}. \tag{40}$$

The continuity conditions (33) between the two layers, can be written as

$$\boldsymbol{G}\boldsymbol{y}(r_m) + \boldsymbol{H}\boldsymbol{z}(r_m) = \boldsymbol{0}, \tag{41}$$

where $r_m = r_i^{(1)} + h^{(1)}$ and matrices $\boldsymbol{G}$ and $\boldsymbol{H}$ are defined as

$$\boldsymbol{G} = \begin{bmatrix} G_{11} & G_{12} & G_{13} & G_{14} \\ G_{21} & G_{22} & G_{23} & 0 \\ G_{31} & 0 & 0 & 0 \\ G_{41} & G_{42} & 0 & 0 \end{bmatrix}, \quad \boldsymbol{H} = \begin{bmatrix} H_{11} & H_{12} & H_{13} & H_{14} \\ H_{21} & H_{22} & H_{23} & 0 \\ H_{31} & 0 & 0 & 0 \\ H_{41} & H_{42} & 0 & 0 \end{bmatrix}. \tag{42}$$

It is now convenient to rearrange the four solutions of (36): two for the first layer, $\boldsymbol{y}^I$, $\boldsymbol{y}^{II}$, and two for the second layer, $\boldsymbol{z}^I$, $\boldsymbol{z}^{II}$, [these solutions already satisfy the boundary conditions (39), but still not the interface conditions (42)] into two matrices sharing the common structure

$$\begin{bmatrix} *_1^I & *_1^{II} \\ *_2^I & *_2^{II} \\ *_3^I & *_3^{II} \\ *_4^I & *_4^{II} \end{bmatrix} \tag{43}$$

(where the symbol $*$ stands for either y or z) and defining the so-called compound matrices. Moreover, we introduce the vectors ϕ_i^y $(i = 1, \ldots, 6)$ and ϕ_i^z $(i = 1, \ldots, 6)$ collecting the components of the minors of matrices (43) as

$$\begin{aligned} \phi_1^* &= *_1^I *_2^{II} - *_2^I *_1^{II}, \quad \phi_4^* = *_2^I *_3^{II} - *_3^I *_2^{II}, \\ \phi_2^* &= *_1^I *_3^{II} - *_3^I *_1^{II}, \quad \phi_5^* = *_2^I *_4^{II} - *_4^I *_2^{II}, \\ \phi_3^* &= *_1^I *_4^{II} - *_4^I *_1^{II}, \quad \phi_6^* = *_3^I *_4^{II} - *_4^I *_3^{II}. \end{aligned} \tag{44}$$

With the definitions (43) and (44), the differential problem (36) can be shown [Ng and Reid 1979a] to be equivalent to the new problem

$$\left(\boldsymbol{\phi}^y\right)' = \boldsymbol{P}^A \boldsymbol{\phi}^y, \quad \left(\boldsymbol{\phi}^z\right)' = \boldsymbol{P}^B \boldsymbol{\phi}^z, \tag{45}$$

where, introducing the symbol $\square$, equal to A (to B) for $\boldsymbol{\phi}^y$ (for $\boldsymbol{\phi}^z$), we define

$$\boldsymbol{P}^{\square} = \begin{bmatrix} 0 & 1 & 0 & 0 & 0 & 0 \\ 0 & 0 & 1 & 1 & 0 & 0 \\ \square_{42} & \square_{43} & \square_{44} & 0 & 1 & 0 \\ 0 & 1 & 0 & 0 & 1 & 0 \\ -\square_{41} & 0 & 0 & \square_{43} & \square_{44} & 1 \\ 0 & -\square_{41} & 0 & -\square_{42} & 0 & \square_{44} \end{bmatrix}. \tag{46}$$

The system of differential equations (45) has to be solved using a Runge–Kutta (4,5) numerical method (we have used Matlab version 7.9) to determine the compound matrices $\boldsymbol{\phi}^y$ and $\boldsymbol{\phi}^z$.

The solution of the bifurcation problem can be written as a linear combination of the solutions $\boldsymbol{y}^I$, $\boldsymbol{y}^{II}$, $\boldsymbol{z}^I$, and $\boldsymbol{z}^{II}$,

$$\boldsymbol{y} = \xi_1 \boldsymbol{y}^I + \xi_2 \boldsymbol{y}^{II}, \quad \boldsymbol{z} = \xi_3 \boldsymbol{z}^I + \xi_4 \boldsymbol{z}^{II}, \tag{47}$$

where the arbitrary coefficients ξ_i $(i = 1, \ldots, 4)$, which set the amplitude of the bifurcation mode, remain undefined in a linearized analysis. The conditions at the internal interface (41) can be recast as

$$\boldsymbol{M}\boldsymbol{\xi} = \boldsymbol{0}, \quad \text{with } [\boldsymbol{\xi}] = [\xi_1 \;\; \xi_2 \;\; \xi_3 \;\; \xi_4]^T, \tag{48}$$

where

$$\boldsymbol{M} = \begin{bmatrix} \left(\boldsymbol{G}\boldsymbol{y}^I\right)_1 & \left(\boldsymbol{G}\boldsymbol{y}^{II}\right)_1 & \left(\boldsymbol{H}\boldsymbol{z}^I\right)_1 & \left(\boldsymbol{H}\boldsymbol{z}^{II}\right)_1 \\ \left(\boldsymbol{G}\boldsymbol{y}^I\right)_2 & \left(\boldsymbol{G}\boldsymbol{y}^{II}\right)_2 & \left(\boldsymbol{H}\boldsymbol{z}^I\right)_2 & \left(\boldsymbol{H}\boldsymbol{z}^{II}\right)_2 \\ \left(\boldsymbol{G}\boldsymbol{y}^I\right)_3 & \left(\boldsymbol{G}\boldsymbol{y}^{II}\right)_3 & \left(\boldsymbol{H}\boldsymbol{z}^I\right)_3 & \left(\boldsymbol{H}\boldsymbol{z}^{II}\right)_3 \\ \left(\boldsymbol{G}\boldsymbol{y}^I\right)_4 & \left(\boldsymbol{G}\boldsymbol{y}^{II}\right)_4 & \left(\boldsymbol{H}\boldsymbol{z}^I\right)_4 & \left(\boldsymbol{H}\boldsymbol{z}^{II}\right)_4 \end{bmatrix}, \tag{49}$$

so that the bifurcation condition, depending on the bending half-angle $\bar{\theta}$, the undeformed aspect ratios l_0/h_0 and $h_0^{(1)}/h_0^{(2)}$, and the stiffness ratio $\mu_0^{(1)}/\mu_0^{(2)}$, becomes

$$\det(\boldsymbol{M}) = 0. \tag{50}$$

Condition (50) can be rewritten as the sum of 2×2-determinants as

$$\sum_{i=0}^{1}(-1)^i\left\{\begin{vmatrix}M_{1+i,1} & M_{1+i,2}\\ M_{41} & M_{42}\end{vmatrix}\begin{vmatrix}M_{2-i,3} & M_{2-i,4}\\ M_{33} & M_{34}\end{vmatrix}-\begin{vmatrix}M_{2+i,1} & M_{2+i,2}\\ M_{11} & M_{12}\end{vmatrix}\begin{vmatrix}M_{3-i,3} & M_{3-i,4}\\ M_{43} & M_{44}\end{vmatrix}\right.$$
$$\left.-\begin{vmatrix}M_{2+2i,1} & M_{2+2i,2}\\ M_{31} & M_{32}\end{vmatrix}\begin{vmatrix}M_{4-2i,3} & M_{4-2i,4}\\ M_{13} & M_{14}\end{vmatrix}\right\}=0. \quad (51)$$

The determinants can be expressed in terms of the compound matrices $\boldsymbol{\phi}^y$ and $\boldsymbol{\phi}^z$ as

$$\begin{vmatrix}M_{k1} & M_{k2}\\ M_{l1} & M_{l2}\end{vmatrix}= (G_{k1}G_{l2}-G_{k2}G_{l1})\phi_1^y+(G_{k1}G_{l3}-G_{k3}G_{l1})\phi_2^y+(G_{k1}G_{l4}-G_{k4}G_{l1})\phi_3^y$$
$$+(G_{k2}G_{l3}-G_{k3}G_{l2})\phi_4^y+(G_{k2}G_{l4}-G_{k4}G_{l2})\phi_5^y+(G_{k3}G_{l4}-G_{k4}G_{l3})\phi_6^y \quad (52)$$

and

$$\begin{vmatrix}M_{k3} & M_{k4}\\ M_{l3} & M_{l4}\end{vmatrix}= (H_{k1}H_{l2}-H_{k2}H_{l1})\phi_1^z+(H_{k1}H_{l3}-H_{k3}H_{l1})\phi_2^z+(H_{k1}H_{l4}-H_{k4}H_{l1})\phi_3^z$$
$$+(H_{k2}H_{l3}-H_{k3}H_{l2})\phi_4^z+(H_{k2}H_{l4}-H_{k4}H_{l2})\phi_5^z+(H_{k3}H_{l4}-H_{k4}H_{l3})\phi_6^z, \quad (53)$$

where the indices k and l take the values corresponding to the representation (51).

Once the undeformed aspect ratios l_0/h_0 and $h_0^{(1)}/h_0^{(2)}$ and the stiffness ratio $\mu_0^{(1)}/\mu_0^{(2)}$ have been fixed, the bifurcation condition (50), through representation (51), becomes a function of the bending half-angle $\bar{\theta}$ only, to be solved numerically (we have used the function "fzero" of Matlab). An example of the advantage related to the use of the compound matrix method over the usual determinantal method is reported in Figure 2, where $\det(\boldsymbol{M})$ is plotted as a function of $\bar{\theta}$ for a stiff case, in which the superiority of the former approach is evident (note the spurious oscillations of the determinantal method). In this

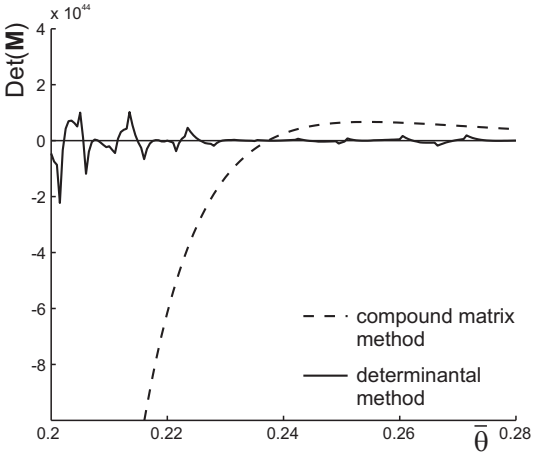

Figure 2. The compound matrix method (dashed line) against the determinantal method (solid line): $\det(\boldsymbol{M})$ is evaluated at different angles $\bar{\theta}$, for l_0/h_0 =0.1, $h_0^{(1)}/h_0^{(2)}$ = (1 mm)/(5 mm) and $\mu_0^{(1)}/\mu_0^{(2)} = (7\,\mathrm{N/mm^2})/(1\,\mathrm{N/mm^2})$. Bifurcation corresponds to the vanishing of $\det(\boldsymbol{M})$; note the spurious oscillations of the latter method.

particular case, the 2-norm condition number of the matrix $\boldsymbol{M}$ is equal to 9.37×10^{27}, a value confirming that the matrix is bad conditioned.

4. Bifurcations of a two-layer system

Results for bifurcation of bent configurations for bilayers are shown in Figure 3, in terms of critical half-angle $\bar{\theta}_{cr}$ (upper graphs) and critical stretch $\lambda_{cr}(r_i^{(1)})$ at the compressed side of the specimen

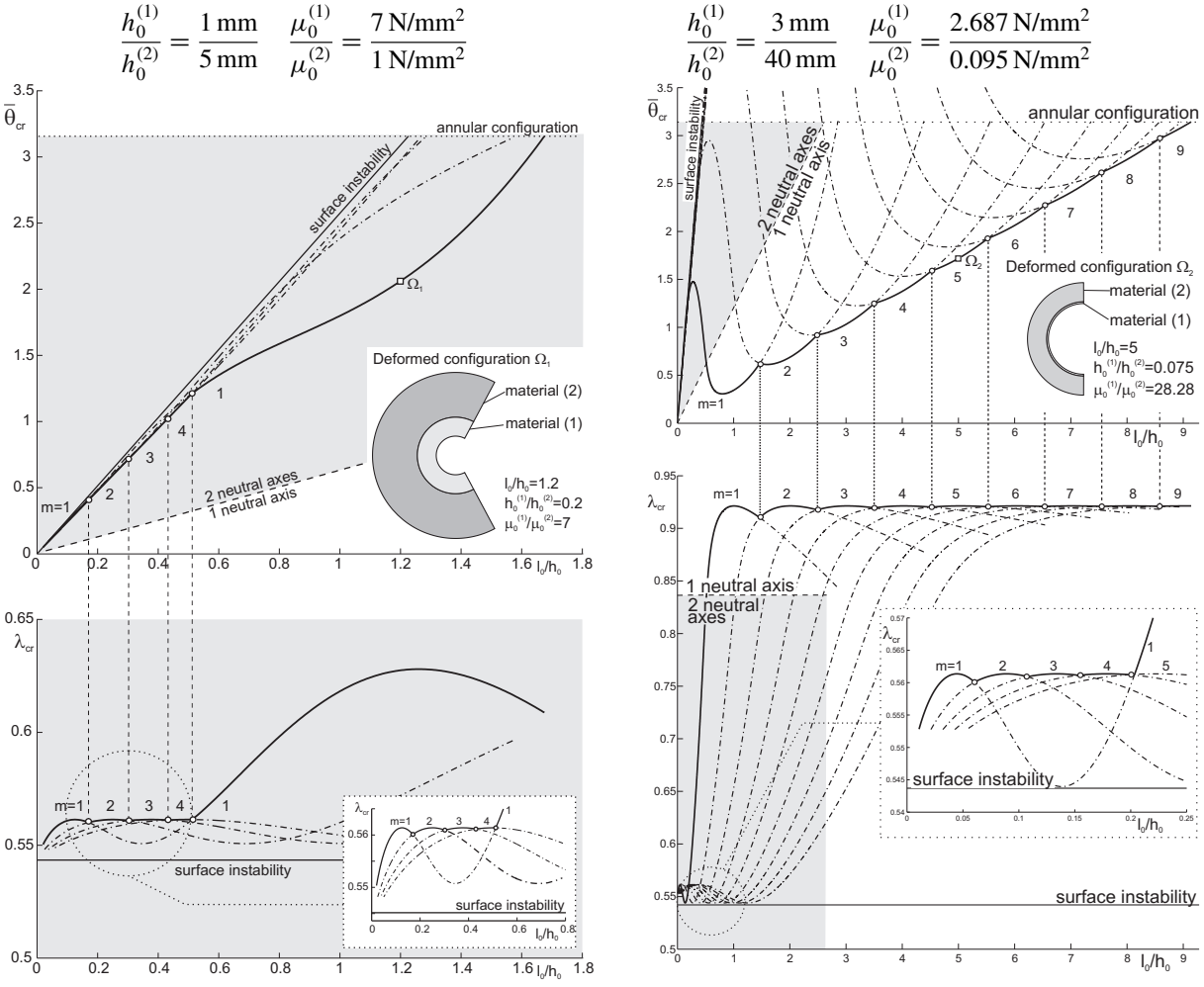

Figure 3. Critical angle $\bar{\theta}_{cr}$ and critical stretch λ_{cr} (evaluated at the internal boundary, $r = r_i^{(1)}$) versus aspect ratio l_0/h_0 for a Mooney–Rivlin bilayer coated with a stiff layer and subject to bending with $h_0^{(1)}/h_0^{(2)}$ and $\mu_0^{(1)}/\mu_0^{(2)}$ as indicated above the graphs. The stiff layer is located at the side in compression. In each plot, a small circle denotes a transition between two integer values of m (the parameter which sets the circumferential wavenumber). In the lower plots, the insert contains a magnification of the region where bifurcations occur at low l_0/h_0. Two neutral axes occur in the region marked gray.

(lower graphs) as functions of the global aspect ratio, that is, the initial length divided by the initial total thickness. The ratios between the thicknesses and the shear coefficients μ_0 of the layers are (1 mm)/(5 mm) and (7 N/mm^2)/(1 N/mm^2) for the left half of Figure 3, and (3 mm)/(40 mm) and (2.687 N/mm^2)/(0.095 N/mm^2) for the right half. The various curves reported in the figure represent solutions corresponding to different bifurcation modes, singled out by the circumferential wavenumber m. The mode visible in an experiment is that corresponding to the lower value of the critical half-angle, $\bar{\theta}_{cr}$, or to the higher value of critical stretch at the compressed side, λ_{cr}. Note that the gray zone represents the range of aspect ratios and bending half-angle for which two neutral axes occur.

Within the set of aspect ratios and stiffness contrast analyzed in the left part of Figure 3, a bifurcation only appears when two neutral axes have been formed, while it may occur when two or one neutral axes are present in the right half of the figure. In all cases analyzed, including Figure 3, we have found that the gray zone in the $\bar{\theta}_{cr}$–l_0/h_0 graphs is bounded by a straight line, becoming a horizontal line in the λ_{cr}–l_0/h_0 representation. An explanation for this fact is given in Appendix C.

The special feature emerging from Figure 3, left (and not found within the set of parameters and geometries investigated in [Roccabianca et al. 2010]) is that the mode $m = 1$ of bifurcation becomes the critical mode for a sufficiently high slenderness, so that here long-wavelength bifurcations (corresponding to small m) become well-separated from surface modes (corresponding to high m) and thus fully visible. This feature is also present in Figure 3, right, which has been produced with values of parameters corresponding to commercially available rubbers (and tested by us; see Appendix B). In this way it has been possible to produce the two samples shown in Figures 1 and 4, differing only in the aspect ratio (taken equal to 2 for the sample shown in Figure 1 and 1.5 for that shown in Figure 4) and evidencing long-wavelength bifurcation modes.

The progression of bending is shown in Figure 4, referred to a 64.5 mm × 3 mm × 150 mm rubber strip glued to a 64.5 mm × 40 mm × 150 mm neoprene plate (in which the larger dimension is that out-of-plane, taken sufficiently large, 150 mm, to simulate the plane strain condition). At a certain stage of finite bending, namely at a certain bending half-angle $\bar{\theta}_{cr}$, a long-wavelength mode can be detected to appear on the surface of the sample (Figure 4, right), which *qualitatively* confirms our findings.

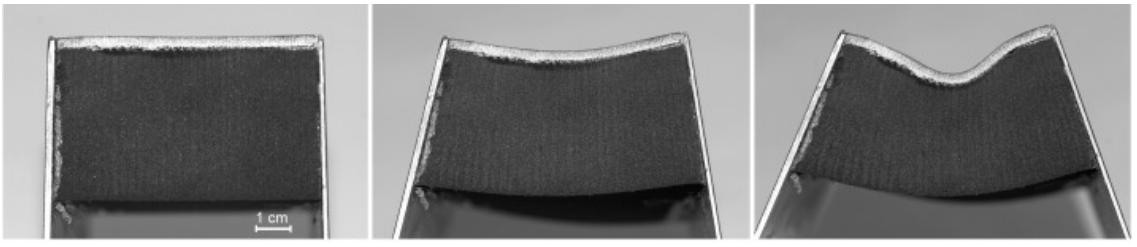

Figure 4. Progressive bending of a two-layer rubber block (undeformed configuration is shown on the left, a bent configuration in the center), evidencing bifurcation with long-wavelength bifurcation modes (shown on the right). Stiffness and thickness ratios between layers are (2.687 N/mm^2)/(0.095 N/mm^2) and (3 mm)/(40 mm), respectively. The stiff layer (64.5 mm × 3 mm × 150 mm, made up of natural rubber, marked with a white pencil on the sample) is at the compressive side and coats a neoprene layer (64.5 mm × 40 mm × 150 mm).

From a quantitative point of view, the critical half-angle for bifurcation results from modeling to be equal to 39.40° for the sample shown in Figure 1 and 35.49° for that shown in Figure 4, values that are definitely higher than those found experimentally (30.00° for the former sample and 21.00° for the latter). The fact that the theoretical predictions correspond to bifurcation angles larger than those observed experimentally is also common to all previous experiments [Gent and Cho 1999; Roccabianca et al. 2010] and can be explained as the usual effect of imperfections (so that for instance the bending mode associated with the Euler buckling is always experimentally observed to become visible before the achievement of the critical load). The fact that the discrepancy between theoretical and experimental values is larger in the cases reported in the present article can be motivated in terms of the effect of the different *sensitivity* to imperfections. In fact, short-wavelength undulations introduced in the reference configuration begin to amplify and to become visible much closer to the bifurcation threshold than long-wavelength imperfections, a feature demonstrated through finite element numerical simulations [Roccabianca 2011].

5. Conclusions

Incremental bifurcations emanating from a finitely bent configuration of an elastic incompressible multi-layered block have been reconsidered after the article [Roccabianca et al. 2010]. It has been shown that the presence of two neutral axes is linked to the possibility of finding long-wavelength bifurcation modes well-separated from (short-wavelength) surface modes, a circumstance which was pointed out without proof in that article and is now definitely demonstrated. Since the equations governing the bifurcation become stiff (specially when more than one neutral axis is present), the treatment of the computational problem has been possible only through an use of the compound matrix method. Our findings have been substantiated by qualitative experiments, giving full evidence to long-wavelength modes.

Appendix A. Components of the compound matrices in (38), (40), (42), and (46)

$$A_{41}(r)=\frac{(n^2-1)(F^{(1)}-rF^{(1)}_{,r}-n^2E^{(1)})}{C^{(1)}r^4},\quad A_{42}(r)=\frac{2F^{(1)}-(rF^{(1)}+2rn^2D^{(1)})_{,r}}{C^{(1)}r^3},$$
$$A_{43}(r)=\frac{2n^2D^{(1)}-(rF^{(1)})_{,r}-4F^{(1)}}{C^{(1)}r^2},\qquad A_{44}(r)=-2\frac{F^{(1)}+2C^{(1)}}{C^{(1)}r}.$$

$$B_{41}(r)=\frac{(n^2-1)(F^{(2)}-rF^{(2)}_{,r}-n^2E^{(2)})}{C^{(2)}r^4},\quad B_{42}(r)=\frac{2F^{(2)}-(rF^{(2)}+2rn^2D^{(2)})_{,r}}{C^{(2)}r^3},$$
$$B_{43}(r)=\frac{2n^2D^{(2)}-(rF^{(2)})_{,r}-4F^{(2)}}{C^{(2)}r^2},\qquad B_{44}(r)=-2\frac{F^{(2)}+2C^{(2)}}{C^{(2)}r}.$$

$$C_{11}=F^{(1)}(n^2-1),\qquad C_{12}=r_i[F^{(1)}-n^2(2D^{(1)}+C^{(1)})],\qquad C_{13}=r_i^2(F^{(1)}+3C^{(1)}),$$
$$D_{11}=F^{(2)}(n^2-1),\qquad D_{12}=r_e[F^{(2)}-n^2(2D^{(2)}+C^{(2)})],\qquad D_{13}=r_e^2(F^{(2)}+3C^{(2)}),$$
$$C_{14}=r_i^3C^{(1)},\qquad C_{21}=n^2-1,\qquad C_{22}=r_i,\qquad C_{31}=r_i^2,$$
$$D_{14}=r_e^3C^{(2)},\qquad D_{21}=n^2-1,\qquad D_{22}=r_e,\qquad D_{23}=r_e^2.$$

$$
\begin{aligned}
&G_{11} = F^{(1)}(n^2-1), && G_{12} = r_m[F^{(1)} - n^2(2D^{(1)} + C^{(1)} - T_r^{(1)})],\\
&H_{11} = F^{(2)}(1-n^2), && H_{12} = r_m[n^2(2D^{(2)} + C^{(2)} - T_r^{(2)}) - F^{(2)}],\\
&G_{13} = r_m^2(F^{(1)} + 3C^{(1)}), && G_{14} = r_m^3 C^{(1)}, \quad G_{21} = (n^2-1)(C^{(1)} - T_r^{(1)}),\\
&H_{13} = -r_m^2(F^{(2)} + 3C^{(2)}), && H_{14} = -r_m^3 C^{(2)}, \quad H_{21} = (1-n^2)(C^{(2)} - T_r^{(2)}),\\
&G_{22} = r_m(C^{(1)} + T_r^{(1)}), && G_{23} = r_m^2 C^{(1)}, \quad G_{31} = 1, \quad G_{41} = 1, \quad G_{42} = r_m,\\
&H_{22} = -r_m(C^{(2)} + T_r^{(2)}), && H_{23} = -r_m^2 C^{(2)}, \quad H_{31} = -1, \quad H_{41} = -1, \quad H_{42} = -r_m.
\end{aligned}
$$

$$
\begin{aligned}
&P_{31}^A = \frac{2F^{(1)} - (rF^{(1)} + 2rn^2D^{(1)})_{,r}}{C^{(1)}r^3}, && P_{32}^A = \frac{2n^2D^{(1)} - (rF^{(1)})_{,r} - 4F^{(1)}}{C^{(1)}r^2}, && P_{33}^A = \frac{-2(F^{(1)} + 2C^{(1)})}{C^{(1)}r},\\
&P_{51}^A = \frac{(1-n^2)(F^{(1)} - rF_{,r}^{(1)} - n^2E^{(1)})}{C^{(1)}r^4}, && P_{54}^A = \frac{2n^2D^{(1)} - (rF^{(1)})_{,r} - 4F^{(1)}}{C^{(1)}r^2}, && P_{55}^A = \frac{-2(F^{(1)} + 2C^{(1)})}{C^{(1)}r},\\
&P_{62}^A = \frac{(1-n^2)(F^{(1)} - rF_{,r}^{(1)} - n^2E^{(1)})}{C^{(1)}r^4}, && P_{64}^A = \frac{(rF^{(1)} + 2rn^2D^{(1)})_{,r} - 2F^{(1)}}{C^{(1)}r^3}, && P_{66}^A = \frac{-2(F^{(1)} + 2C^{(1)})}{C^{(1)}r}.
\end{aligned}
$$

$$
\begin{aligned}
&P_{31}^B = \frac{2F^{(2)} - (rF^{(2)} + 2rn^2D^{(2)})_{,r}}{C^{(2)}r^3}, && P_{32}^B = \frac{2n^2D^{(2)} - (rF^{(2)})_{,r} - 4F^{(2)}}{C^{(2)}r^2}, && P_{33}^B = \frac{-2(F^{(2)} + 2C^{(2)})}{C^{(2)}r},\\
&P_{51}^B = \frac{(1-n^2)(F^{(2)} - rF_{,r}^{(2)} - n^2E^{(2)})}{C^{(2)}r^4}, && P_{54}^B = \frac{2n^2D^{(2)} - (rF^{(2)})_{,r} - 4F^{(2)}}{C^{(2)}r^2}, && P_{55}^B = \frac{-2(F^{(2)} + 2C^{(2)})}{C^{(2)}r},\\
&P_{62}^B = \frac{(1-n^2)(F^{(2)} - rF_{,r}^{(2)} - n^2E^{(2)})}{C^{(2)}r^4}, && P_{64}^B = \frac{(rF^{(2)} + 2rn^2D^{(2)})_{,r} - 2F^{(2)}}{C^{(2)}r^3}, && P_{66}^B = \frac{-2(F^{(2)} + 2C^{(2)})}{C^{(2)}r}.
\end{aligned}
$$

Appendix B. Experimental determination of the stiffness coefficient μ_0 of the employed materials

In our qualitative experiments to detect bifurcation, we have imposed finite bending to bilayered systems made up of a natural rubber strip (3 mm thick) and a neoprene block (40 mm thick). The bilayer is obtained by gluing the neoprene block to the natural rubber strip (we have used ethyl cyanoacrylate, Pattex©).

Four dog-bone-shaped standard ISO 5277-1/1BA 30 mm × 5 mm specimens have been sampled from the two materials to characterize them in terms of Mooney–Rivlin model. Result of the tests (performed at room temperature with a Messphysik Midi 10 testing machine equipped with Doli Edc 222 acquisition and control electronics) are shown in Figure 5, in terms of true stress versus stretch. The selected ranges of stress and stretch for the tests correspond to the values expected in the bending experiments.

In the plots, the interpolation with the Mooney–Rivlin material (which provides a nearly linear response at the stretch under consideration) selected for the calculations is also included. The least square method provides for the natural rubber $c_1^{(\text{natrub})} = 0.007\,\text{N/mm}^2$, $c_2^{(\text{natrub})} = 2.68\,\text{N/mm}^2$ (corresponding to $\mu_0^{(\text{natrub})} \simeq 2.687\,\text{N/mm}^2$) and for the neoprene $c_1^{(\text{neopr})} = 0.09\,\text{N/mm}^2$, $c_2^{(\text{neopr})} = 0.005\,\text{N/mm}^2$, giving $\mu_0^{(\text{neopr})} \simeq 0.095\,\text{N/mm}^2$.

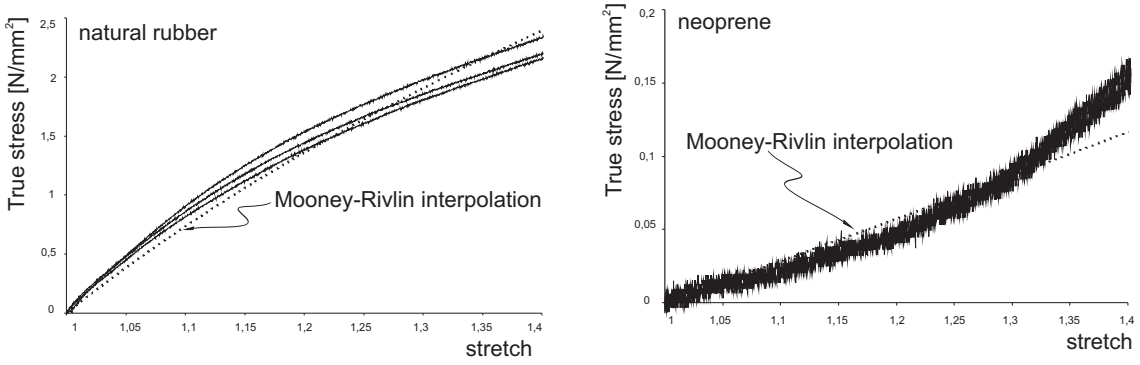

Figure 5. Uniaxial tests and material characterization of the natural rubber and the neoprene plate employed for the specimens to be subject to bending. Dotted curves represent Mooney–Rivlin interpolations employed in the analysis.

Appendix C. A justification of the fact that the region in which two neutral axes are present is bounded by a straight line in Figure 3

We provide a justification of the finding that, when two neutral axes occur in a bilayer, the stretch (at the compressed side) is independent of the global aspect ratio l_0/h_0, so that the gray zone (corresponding to the presence of two neutral axes) is bounded by a horizontal (inclined) line in the λ_{cr}–l_0/h_0 (in the $\bar{\theta}_{cr}$–l_0/h_0) representation, Figure 3.

The explanation of this effect is based on two observations:

i. During progressive bending of a bilayer with the stiff layer under compression, one neutral axis is present from the beginning of the deformation within the soft layer, while the second neutral axis always nucleates at the interface between the two layers (and then moves in the stiff layer).

ii. When the second neutral axis nucleates, the radial Cauchy stress T_r at the interface between layers takes a value independent of the initial aspect ratio l_0/h_0. We can therefore operate on a single layer by imposing, in addition to the usual bending, a pressure P^{ext} at one of its external sides (of initial length l_0) to correspond to the radial stress at the interface between layers. In particular, we can apply P^{ext} at the side where the longitudinal stretch is greater than 1.

To operate in dimensionless form, we introduce, from (2) and (4), the kinematic unknowns

$$\bar{\alpha} = \frac{2\bar{\theta}}{a}, \quad \bar{r} = \frac{r}{h_0}, \quad \bar{h} = \frac{h}{h_0}, \tag{C.1}$$

where $a = l_0/h_0$ is the aspect ratio of the undeformed configuration. The internal and external nondimensional radii, from (1), are

$$\bar{r}_i = \frac{a}{2\bar{\theta}\bar{h}} - \frac{\bar{h}}{2}, \quad \bar{r}_e = \bar{r}_i + \bar{h}. \tag{C.2}$$

As we want to write the bending problem in terms of the variable $\lambda_i = \lambda(\bar{r}_i)$, we calculate $\bar{\theta}$ as a function of a, $\bar{h}$ and λ_i, so that $(4)_2$ gives

$$\bar{\theta} = \frac{a}{\bar{h}} \left(\frac{1}{\bar{h}} - \lambda_i \right), \tag{C.3}$$

and the condition $\lambda_e = \lambda(\bar{r}_e)$ becomes

$$\lambda_e = \frac{2}{\bar{h}} - \lambda_i. \tag{C.4}$$

The boundary conditions for the layer under consideration are now

$$T_r(\bar{r}_i) = 0, \quad T_r(\bar{r}_e) = P^{\text{ext}}, \tag{C.5}$$

where

$$T_r = \frac{\mu_0}{2} \left(\lambda^2 + \frac{1}{\lambda^2} \right) + \gamma,$$

can be written from $(10)_1$. Equation $(C.5)_2$ provides the coefficient γ in the form

$$\gamma = P^{\text{ext}} - \frac{\mu_0}{2} \left(\lambda_e^2 + \frac{1}{\lambda_e^2} \right), \tag{C.6}$$

while, on the other hand, $(C.5)_1$ is equivalent to

$$\lambda_i^2 + \frac{1}{\lambda_i^2} + 2\frac{P^{\text{ext}}}{\mu_0} - \left[\left(\frac{2}{\bar{h}} - \lambda_i \right)^2 + \left(\frac{2}{\bar{h}} - \lambda_i \right)^{-2} \right] = 0, \tag{C.7}$$

from which it is clear that the unknown $\bar{h}$ is independent of a (but remains dependent on λ_i, μ_0, and P^{ext}). Therefore, since a neutral axis corresponds to

$$T_\theta(\bar{r}_e) = 0, \tag{C.8}$$

equations $(10)_2$, (C.6), and (C.4) show that the neutral axis condition is independent of a, so that the solution in terms of λ_i becomes only a function of μ_0 and P^{ext}.

References

[Anturkar et al. 1992] N. R. Anturkar, T. C. Papanastasiou, and J. O. Wilkes, "Compound matrix method for eigenvalue problems in multiple connected domains", *Comm. Appl. Numer. Methods* **8**:11 (1992), 811–818.

[Backus and Gilbert 1967] G. E. Backus and J. F. Gilbert, "Numerical applications of a formalism for geophysical inverse problems", *Geophys. J. Roy. Astron. Soc.* **13** (1967), 247–276.

[Benallal et al. 1993] A. Benallal, R. Billardon, and G. Geymonat, "Bifurcation and localization in rate-independent materials: some general considerations", pp. 1–44 in *Bifurcation and stability of dissipative systems* (Udine, 1991), edited by Q. S. Nguyen, CISM Courses and Lectures **327**, Springer, Vienna, 1993.

[Coman and Destrade 2008] C. D. Coman and M. Destrade, "Asymptotic results for bifurcations in pure bending of rubber blocks", *Quart. J. Mech. Appl. Math.* **61**:3 (2008), 395–414.

[Destrade et al. 2009] M. Destrade, A. Ní Annaidh, and C. D. Coman, "Bending instabilities of soft biological tissues", *Int. J. Solids Struct.* **46** (2009), 4322–4330.

[Destrade et al. 2010] M. Destrade, M. D. Gilchrist, J. A. Motherway, and J. G. Murphy, "Bimodular rubber buckles early in bending", *Mech. Mater.* **42** (2010), 469–476.

[Dryburgh and Ogden 1999] G. Dryburgh and R. W. Ogden, "Bifurcation of an elastic surface-coated incompressible isotropic elastic block subject to bending", *Z. Angew. Math. Phys.* **50**:5 (1999), 822–838.

[Gei and Ogden 2002] M. Gei and R. W. Ogden, "Vibration of a surface-coated elastic block subject to bending", *Math. Mech. Solids* **7**:6 (2002), 607–628.

[Gent 2005] A. N. Gent, "Elastic instabilities in rubber", *Int. J. Nonlinear Mech.* **40** (2005), 165–175.

[Gent and Cho 1999] A. N. Gent and I. S. Cho, "Surface instabilities in compressed or bent rubber blocks", *Rubber Chem. Technol.* **72** (1999), 253–262.

[Haughton 1999] D. M. Haughton, "Flexure and compression of incompressible elastic plates", *Internat. J. Engrg. Sci.* **37**:13 (1999), 1693–1708.

[Haughton and Orr 1995] D. M. Haughton and A. Orr, "On the eversion of incompressible elastic cylinders", *Int. J. Nonlinear Mech.* **30** (1995), 81–95.

[Hill and Hutchinson 1975] R. Hill and J. W. Hutchinson, "Bifurcation phenomena in the plane tension test", *J. Mech. Phys. Solids* **23**:4-5 (1975), 239–264.

[Lindsay 1992] K. A. Lindsay, "The application of compound matrices to convection problems in multi-layered continua", *Math. Models Methods Appl. Sci.* **2**:2 (1992), 121–141.

[Lindsay and Rooney 1992] K. A. Lindsay and C. E. Rooney, "A note on compound matrices", *J. Comput. Phys.* **103**:2 (1992), 472–477.

[Ng and Reid 1979a] B. S. Ng and W. H. Reid, "An initial value method for eigenvalue problems using compound matrices", *J. Comput. Phys.* **30**:1 (1979), 125–136.

[Ng and Reid 1979b] B. S. Ng and W. H. Reid, "A numerical method for linear two-point boundary value problems using compound matrices", *J. Comput. Phys.* **33**:1 (1979), 70–85.

[Ng and Reid 1985] B. S. Ng and W. H. Reid, "The compound matrix method for ordinary differential systems", *J. Comput. Phys.* **58**:2 (1985), 209–228.

[Rivlin 1949] R. S. Rivlin, "Large elastic deformations of isotropic materials, V: The problem of flexure", *Proc. Roy. Soc. London. Ser. A.* **195** (1949), 463–473.

[Roccabianca 2011] S. Roccabianca, *Multilayered structures under large bending: finite solution and bifurcation analysis*, PhD Thesis, University of Trento, 2011.

[Roccabianca et al. 2010] S. Roccabianca, M. Gei, and D. Bigoni, "Plane strain bifurcations of elastic layered structures subject to finite bending: theory versus experiments", *IMA J. Appl. Math.* **75**:4 (2010), 525–548.

[Triantafyllidis 1980] N. Triantafyllidis, "Bifurcation phenomena in pure bending", *J. Mech. Phys. Solids* **28**:3-4 (1980), 221–245.

[Yiantsios and Higgins 1988] S. G. Yiantsios and B. G. Higgins, "Numerical solution of eigenvalue problems using the compound matrix method", *J. Comput. Phys.* **74**:1 (1988), 25–40.

Received 29 May 2010. Revised 22 Oct 2010. Accepted 22 Oct 2010.

SARA ROCCABIANCA: sara.roccabianca@yale.edu
Department of Biomedical Engineering, Yale University, New Haven, CT 06511, United States

DAVIDE BIGONI: bigoni@ing.unitn.it
University of Trento, Department of Mechanical and Structural Engineering, Via Mesiano 77, I-38123 Trento, Italy

MASSIMILIANO GEI: mgei@ing.unitn.it
University of Trento, Department of Mechanical and Structural Engineering, Via Mesiano 77, I-38123 Trento, Italy